J. Fluid Mech. (1976), *vol.* 77, *part* 1, *pp.* 153–175
Printed in Great Britain

Roll-cell instabilities in rotating laminar and turbulent channel flows

By DIETRICH K. LEZIUS† AND JAMES P. JOHNSTON

Department of Mechanical Engineering, Stanford University

(Received 10 February 1975)

The stability of laminar and turbulent channel flow is examined for cases where Coriolis forces are introduced by steady rotation about an axis perpendicular to the plane of mean flow. Linearized equations of motion are derived for small disturbances of the Taylor type. Conditions for marginal stability in laminar Couette and Poiseuille flow correspond, in part, to the analogous solutions of buoyancy-driven convection instabilities in heated fluid layers, and to those of Taylor instabilities in the flow between rotating cylinders. In plane Poiseuille flow with rotation, the critical disturbance mode occurs at a Reynolds number of $Re_c = 88{\cdot}53$ and rotation number $Ro = 0{\cdot}5$. At higher Reynolds numbers, unstable conditions can exist over the range of rotation numbers given by $0 < Ro < 3$, provided the undisturbed flow remains laminar. A two-layer model is devised to investigate the onset of longitudinal instabilities in turbulent flow. The linear disturbance equations are solved essentially in their laminar form, whereby the velocity gradient of laminar flow is replaced by a numerically computed profile for the gradient of the turbulent mean velocity. The turbulent stress levels in the stable and unstable flow regions are represented by integrated averages of the eddy viscosity. Onset of instability for Reynolds numbers between 6000 and 35 000 is predicted to occur at $Ro = 0{\cdot}022$, a value in remarkable agreement with the experimentally observed appearance of roll instabilities in rotating turbulent channel flow.

1. Introduction

In recent studies of rotating laminar and turbulent channel flow, stabilizing and destabilizing phenomena have been observed that are, in some respects, closely related to the well-known destabilization of the flow between rotating cylinders into Taylor vortex cells. In the flow between rotating cylinders, imbalance between the centrifugal force and the local pressure gradient results in instability with respect to radial fluid exchange. Analogously, the rotating linear shear flow, whose mean vorticity vector is parallel to the rotation vector, becomes unstable when the Coriolis force on a perturbed fluid particle is not balanced by the local pressure gradient across streamlines. The necessary

† Present address: Lockheed Palo Alto Research Laboratory, California.

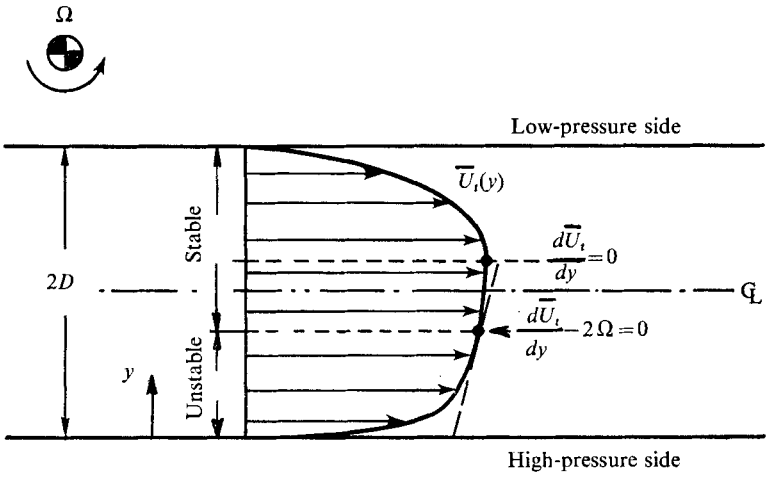

FIGURE 1. Stable and unstable regions in rotating channel flow, indicating the asymmetry of the turbulent mean velocity profile $\overline{U}_t(y)$ when $\Omega > 0$.

conditions leading to instability of the inviscid flow (Bradshaw 1969; Pedley 1969) are satisfied locally when

$$2\Omega(d\overline{U}/dy - 2\Omega) > 0.$$

$d\overline{U}/dy$ is the transverse gradient of the mean velocity, measured in the rotating system; Ω is the rate of angular rotation of the system. (Refer to figures 1 and 14.) The condition above corresponds to Rayleigh's inviscid stability criterion for flow along concentric circular streamlines. It requires a positive radial gradient of circulation for stability of the inviscid flow. Since $-(d\overline{U}/dy - 2\Omega)$ represents the absolute vorticity of the rotating plane flow in inertial co-ordinates, the necessary requirement for instability is satisfied if the absolute vorticity is negative somewhere within the flow. This criterion is not sufficient for predicting instabilities in real fluids, however, since the onset of roll instabilities is delayed by the effects of viscous friction. As will be seen in §4, critical conditions are delayed even further by the effects of turbulent friction. Nevertheless, the inviscid condition remains useful in establishing the potential for local fluid stability in the two wall regions of fully-developed channel flow. The criterion predicts instability near the high-pressure wall for moderate Ω (i.e. $d\overline{U}/dy > 2\Omega > 0$), and stability near the opposite wall, where $d\overline{U}/dy < 0$. The line of neutral stability occurs where vorticity measured in inertial space is zero.

The tendency of two-dimensional laminar and turbulent shear flows with rotation to become unstable to streamwise disturbances of Taylor's type, here denoted as roll cells, has been known for some time. The original observation of this phenomenon was made by Halleen & Johnston (1967), who detected a relatively large-scale, streamwise structure that was embedded in the turbulent flow near the high-pressure wall of a rotating channel apparatus. Subsequent visualization experiments on rotating flow by Lezius & Johnston (1971) showed conclusively the presence of counter-rotating vortex cells when critical angular

rotation rates were exceeded. Near the conditions required for onset of instabilities, the superimposed secondary flow is of small magnitude, and does not significantly disturb the two-dimensionality of the turbulent mean flow. In the supercritical regime (i.e. at rotation rates considerably larger than critical), however, strong nonlinear interaction between the turbulent flow and the instability causes significant three-dimensional distortions. The velocity measurements of Halleen & Johnston (1967) also indicated that, in the subcritical regime (at small rates of rotation in the absence of roll cells), the mean velocity profile of fully-developed turbulent channel flow becomes asymmetrical, as shown in figure 1. The asymmetry arises from the effects of the Coriolis force field upon the mechanisms that produce turbulence energy and Reynolds stress. These features are summarized in Johnston, Halleen & Lezius (1972), and will not be reviewed in detail. Because of their importance to our later consideration of roll-cell instabilities, we mention only that, at high rates of rotation, complete suppression of local turbulence production by the Coriolis field was observed near the low-pressure wall, resulting in a laminar wall layer. Near the high-pressure wall, Coriolis forces tended to further destabilize the turbulent flow by amplifying the rate of turbulence production and local shearing stresses.

In this paper, we shall employ linear theory for disturbances of small magnitude, to predict the onset of longitudinal roll-cell instabilities in laminar and in turbulent channel flow. Hart (1971) presented such an analysis for the laminar case, together with experimental measurements of the critical conditions required for the onset of instabilities. Although Hart's numerically computed stability boundary lies within a region that separates the experimentally observed stable and unstable states, his numerical results predict stability of the flow to higher Reynolds numbers for given angular rotation when compared with the results of our own numerical computations for the marginal stability of laminar Poiseuille flow, and also by comparison with the results of Chandrasekhar (1961*a*, p. 304) for a rotating cylinder. It turns out that the solutions for marginal stability of this type of channel flow are easily derived from Chandrasekhar's eigensolutions to the mathematically analogous disturbance equations for Taylor flow within a small gap, when one expresses the Taylor number in terms of the parameters governing the rotating plane Poiseuille flow.

The analysis for the turbulent case is complicated by the fact that the mean velocity profile and the distribution of turbulent friction become asymmetrical with respect to the channel centre-line when rotation is increased from zero. Since the mean velocity profile determines local stability, and since fluid friction exerts a damping influence on convection instabilities, the effects of asymmetrical profiles for the mean velocity and for the turbulent shear stresses must be included in a realistic analysis. In Lezius & Johnston (1971), predictions of asymmetrical turbulent velocity profiles were successfully based on a variable eddy viscosity model, that received some input from measured data. These features are incorporated into the present analysis, by adopting a two-layer model for the turbulent flow in which the mean velocity varies smoothly; but the turbulent viscosity is represented by an appropriate constant average in each layer.

A question may be raised as to the validity of a linear analysis for small dis-

turbances in a flow that already contains nonlinearly interacting disturbances: i.e. turbulence. In answer, it may be pointed out that any two-dimensional turbulent flow will eventually yield to the application of destabilizing force fields, and develop steady, three-dimensional motions. Since the essential purpose of the stability analysis is to predict the force levels required for this yielding, it is necessary only to describe the apparent resistance of the fluid to sustained shearing motions of small magnitude. In our case, this resistance is represented by a suitable eddy-viscosity model. It is also believed that interference by the turbulent fluctuations with onset of the instability becomes less important if the length scale of the latter is large compared with the length scales of the fluctuating components of the flow. Although the length scales of the turbulent 'eddies' are considerably smaller, over a large portion of the turbulence spectrum, than those of the roll instability, the largest eddies encountered in this flow have length scales approaching $2D$, the scale of the roll cells. Since the turbulence lacks stationary, organized structure, however, it is simply transported with the disturbance, as shown in Johnston *et al.* (1972, figure 12(*b*)). The turbulent mean flow is therefore assumed to be maintained by sufficiently random and homogeneous velocity fluctuations; its stability to Coriolis effects, furthermore, is determined predominantly by the apparent viscosity of the flow, not by the size or structure of the turbulent eddies.

2. Analysis for small disturbances

2.1. *Equations of the basic flow*

The non-dimensional equations of motion of viscous and incompressible plane flow between semi-infinite walls in rotation about a spanwise axis are

$$\frac{\partial u_i}{\partial x_i} = 0, \tag{1}$$

$$\frac{\partial u_i}{\partial t} + u_j \frac{\partial u_i}{\partial x_j} + \begin{bmatrix} -2Ro\,u_2 \\ 2Ro\,u_1 \\ 0 \end{bmatrix} = -\frac{\partial p}{\partial x_i} + \frac{1}{Re}\frac{\partial^2 u_i}{\partial x_j \partial x_j}. \tag{2}$$

(See Lezius & Johnston 1971.) The Coriolis acceleration terms in square brackets result from the vector product $2Ro\,\mathbf{i}_3 \times \mathbf{u}$. In these equations, the Cartesian coordinates are non-dimensionalized by $2D$, whereas the velocity components are scaled upon the integrated average velocity U_m. The effects of centrifugal acceleration are absorbed in the pressure term. (See Johnston *et al.* 1972.) The resulting reduced pressure is then non-dimensionalized by ρU_m^2. The governing parameters of this flow, the Reynolds number and rotation number, are defined by

$$Re = U_m 2D/\nu, \quad Ro = \Omega 2D/U_m. \tag{3,) (4}$$

Using appropriate boundary conditions at the walls, $x_2 = 0$ and $x_2 = 1$, it is readily shown that rotating Couette and Poiseuille flow are identical to solutions of (1) and (2) for $Ro = 0$. In both cases, the basic undisturbed flow remains unaffected by rotation, but the Coriolis acceleration gives rise to a pressure gradient in the x_2 direction $\partial p/\partial x_2 = -2Ro\,u_1$. (5)

2.2. *Linearized disturbance equations*

We are seeking the critical conditions for the onset of infinitesimal disturbances of velocity $\tilde{u}_i$ and pressure $\tilde{p}$, and assume that they are superimposed upon the basic flow, described by U_i and P^*. Instantaneous velocities and pressure are thus written as

$$u_i = U_i + \tilde{u}_i, \quad p = P^* + \tilde{p}. \tag{6), (7}$$

Substituting (6) and (7) into (2), and subtracting the terms of the basic flow which satisfy

$$U_j \frac{\partial U_i}{\partial x_j} + \begin{bmatrix} -2\,Ro\,U_2 \\ 2\,Ro\,U_1 \\ 0 \end{bmatrix} = -\frac{\partial P^*}{\partial x_i} + \frac{1}{Re}\frac{\partial^2 U_i}{\partial x_j \partial x_j} \tag{8}$$

yields the time-dependent disturbance equation

$$\frac{\partial \tilde{u}_i}{\partial t} + (U_j + \tilde{u}_j)\frac{\partial \tilde{u}_i}{\partial x_j} + \tilde{u}_j \frac{\partial U_i}{\partial x_j} + \begin{bmatrix} -2\,Ro\,\tilde{u}_2 \\ 2\,Ro\,\tilde{u}_1 \\ 0 \end{bmatrix} = -\frac{\partial \tilde{p}}{\partial x_i} + \frac{1}{Re}\frac{\partial^2 \tilde{u}_i}{\partial x_j \partial x_j}. \tag{9}$$

Equation (9) is linearized by neglecting products of the disturbances. Furthermore, we limit consideration to two-dimensional, fully-developed channel flow ($U_2 = U_3 = 0$), so that

$$U_j \frac{\partial \tilde{u}_i}{\partial x_j} = U_1 \frac{\partial \tilde{u}_i}{\partial x_1} \quad \text{and} \quad \tilde{u}_j \frac{\partial U_i}{\partial x_j} = \tilde{u}_2 \frac{dU_1}{dx_2} = \tilde{u}_2 U_1'.$$

The latter term is combined with the corresponding rotation terms, to give the linearized disturbance equations in the form

$$\frac{\partial \tilde{u}_i}{\partial t} + U_1 \frac{\partial \tilde{u}_i}{\partial x_1} + \begin{bmatrix} (U_1' - 2\,Ro)\,\tilde{u}_2 \\ 2\,Ro\,\tilde{u}_1 \\ 0 \end{bmatrix} = -\frac{\partial \tilde{p}}{\partial x_i} + \frac{1}{Re}\frac{\partial^2 \tilde{u}_i}{\partial x_j \partial x_j}. \tag{10}$$

The equation of continuity (1) is satisfied by

$$\partial \tilde{u}_i / \partial x_i = 0. \tag{11}$$

Appropriate boundary conditions for channel flow are

$$\tilde{u}_i(0) = \tilde{u}_i(1) = 0. \tag{12}$$

Equations (10)–(12) constitute a complete set for the perturbation velocities $\tilde{u}_i$ and the perturbation pressure field $\tilde{p}$. Depending upon the distribution of U_1' through the fluid layer, the solutions of these equations yield the flow conditions, Re and Ro, for which the assumed disturbance can exist.

We note here the coupling of the x_2 component of the disturbance to the absolute vorticity of the basic flow

$$\xi = -(U_1' - 2\,Ro).$$

It will be shown subsequently that disturbances are not amplified by the Coriolis field in the inviscid flow, unless this quantity is negative over a fluid layer of finite thickness.

2.3. *Roll-cell disturbance modes*

Since the disturbance equations (10) are represented by a set of linear differential equations with constant coefficients, the solutions are sought in terms of normal modes $\exp(i\alpha x_3)$, where α is the spanwise roll frequency. Although general Taylor-type instabilities exhibit streamwise variation in certain supercritical states, linear analysis customarily assumes disturbances without longitudinal modes. In Hart (1971) this assumption was based upon experimental evidence. Rigorous proof was given by Joseph (1966), however, that the lowest critical conditions for longitudinal rolls in Boussinesq fluids (e.g. plane fluid layer heated from below with Couette flow profile) are obtained when the streamwise modes are absent. By physical and, hence, mathematical analogy, this proof also holds for rotating Couette flow; but we assume that it is generally valid for Coriolis-driven disturbances of a larger class of parallel shear flows, including the Poiseuille flow.

The normal-mode description of the disturbance is thus given by

$$[\tilde{u}_i, \tilde{p}] = \tfrac{1}{2}\{[\hat{u}_i(x_2), \hat{p}(x_2)] \exp(i\alpha x_3 + \sigma t) + \text{complex conjugate}\}. \tag{13}$$

$\hat{u}_i$ and $\hat{p}$ are eigenfunctions of the disturbance field; and σ is the inverse time constant of the spanwise mode α. Substitution of (13) into (10) results, after elimination of the pressure and incorporation of (11), in a set of ordinary differential equations for the eigenfunctions of the streamwise and transverse disturbance velocities:

$$[\sigma - Re^{-1}(D^2 - \alpha^2)]\,\hat{u}(y) + (U' - 2Ro)\,\hat{v}(y) = 0, \tag{14}$$

$$[\sigma - Re^{-1}(D^2 - \alpha^2)]\,(D^2 - \alpha^2)\,\hat{v}(y) - \alpha^2 2Ro\,\hat{u}(y) = 0. \tag{15}$$

For convenience, we changed the notation to

$$x_i = [x, y, z], \quad d/dx_2 = D, \quad \hat{u}_1, \hat{u}_2 = \hat{u}, \hat{v} \quad \text{and} \quad U_1' = U'.$$

Appropriate boundary conditions are expressed in (12). Since the spanwise velocity component has been eliminated, an additional condition on $\hat{v}$ can be derived from (11) after substitution of (13). It follows that, at the solid boundaries,

$$\hat{u}(0) = \hat{u}(1) = \hat{v}(0) = \hat{v}(1) = D\hat{v}(0) = D\hat{v}(1) = 0. \tag{16}$$

For the general case, the eigenvalues σ of the problem posed by (14)–(16) give the exponential growth rate of the disturbance mode α for chosen values of Re and Ro. Negative σ, of course, signify a damped disturbance, and hence stability of the flow to the mode α. Since we are interested in marginal stability ($\sigma = 0$), we seek the eigenmodes $\alpha(Re, Ro)$ for which the system of equations has solutions.

3. Dynamically similar solutions

3.1. *Laminar Couette flow*

Hart (1971) pointed out the dynamical similarity between longitudinal roll instabilities in a rotating rectangular channel and convection instabilities in a fluid layer heated differentially from below. Although the frequently observed

hexagonal Bénard cells† of the thermal problem lack direct physical similarity to roll cells of the Taylor type, equivalence of the linearized disturbance equations and boundary conditions yields identical results, in terms of the governing parameters for the onset of instabilities. The neutral stability boundary for Couette flow, in terms of Re and Ro, can thus be calculated from the well-known critical Rayleigh number $Ra = 1708$, computed by Pellew & Southwell (1940). This result was also obtained by Hung, Joseph & Munson (1972), by considering rotating plane Couette flow as a limiting case of Couette flow between rotating cylinders.

It will subsequently be shown that complete physical and dynamical similarity exists between rotating Couette flow and the differentially-heated linear Couette flow, the case considered by Joseph (1966). Since hydrodynamically identical conditions are established in the rotating as well as in the heated flow by the presence of a linearly-varying body force field, identically shaped streamwise roll cells occur when the stability parameter exceeds the value of 1708. The relationship between the corresponding parameters is demonstrated by first combining (14) and (15) into a sixth-order differential equation for the eigenfunction of the $\hat{v}(y)$ component. Incorporating the Couette flow gradient $U' = 2$ produces the result

$$(D^2-\alpha^2-\sigma Re)^2(D^2-\alpha^2)\hat{v}(y)+\alpha^2 4Re^2 Ro(1-Ro)\hat{v}(y) = 0. \tag{17}$$

The boundary conditions are satisfied by

$$\hat{v} = D\hat{v} = (D^2-2\alpha^2-\sigma Re)D^2\hat{v} = 0, \quad y = 0, 1. \tag{18}$$

The equivalent differential equation and boundary conditions for marginally stable disturbances in the thermal problem (indicated by subscript th) have the form

$$(D^2-k_y^2)^3\hat{w}(z)+k_y^2(Ra+Re^2)_{\text{th}}\hat{w}(z) = 0 \tag{19}$$

and

$$\hat{w} = D\hat{w} = (D^2-2k_y^2)D^2\hat{w} = 0, \quad z = 0, 1 \tag{20}$$

(following Joseph 1966). $\hat{w}(z)$ is the eigenfunction of the disturbance component normal to the fluid boundaries. For $Re_{\text{th}} = 0$, the above problem reduces, of course, to that of Bénard convection.

The similarity between the disturbance equations for the rotating and for the heated Couette flow are easily recognized. Thus, the neutrally stable state ($\sigma = 0$) has the corresponding solutions

$$4Re^2Ro(1-Ro) = Ra+Re_{\text{th}}^2 = 1708, \tag{21}$$

with $\alpha_c = k_y = 3{\cdot}1$ for the critical cell number. The lowest critical value of the Reynolds number occurs at $Ro = 0{\cdot}5$ when $Re_c = 41{\cdot}3$. Below Re_c, all disturbance modes are damped, regardless of the value of Ro. This conclusion also carries over by analogy via Joseph's (1966) proof of the impossibility of subcritical unstable states.

† Other possible modes of thermal convection instabilities are linear and concentric roll cells.

The analogies can be further exploited to yield answers to questions of overstability and the range of the stability parameter. These issues were resolved by Chandrasekhar (1961*a*, p. 24) for Bénard convection, with the result that σ can assume only real values, commonly known as the principle of exchange of stabilities. The strictly mathematical proof applies equally to (17) and (18). It is therefore concluded that, in the marginally stable state, longitudinal roll instabilities in rotating Couette flow remain stationary. Since, furthermore, marginally stable solutions to the Rayleigh problem are shown to exist for only positive values of Ra, the solutions of (17) and (18) are limited to the region $Re^2 Ro(1-Ro) > 0$. The expression $Ro(1-Ro)$ is recognized as the non-dimensional form of Rayleigh's discriminant for plane Couette flow, which by the condition that it be positive restricts the range of the allowable rotation number to $0 < Ro < 1$. This requirement, furthermore, establishes the necessary condition that the absolute vorticity, given in non-dimensional co-ordinates by $-2(1-Ro)$, be negative somewhere within the fluid layer for instabilities to occur. In the case of Couette flow, it has a constant negative value throughout. The condition is not sufficient, however. Although reversed rotation $Ro < 0$ introduces more negative vorticity, it obviously violates the requirement that $Re^2 Ro(1-Ro) > 0$. Thus, the latter constraint provides the sufficiency condition for instabilities in an inviscid rotating, plane Couette flow.

3.2. *Laminar Poiseuille flow*

Because of the symmetry of the Poiseuille flow profile, the necessary condition for instabilities (i.e. that the absolute vorticity be negative over a finite region of the flow) is satisfied for certain magnitudes of Ro, regardless of the sense of rotation. When in addition the Rayleigh discriminant has positive values in the same region, instabilities can be expected to occur.

There are two physical analogues to the problem of stability in rotating plane Poiseuille flow: the internally-heated fluid layer considered by Debler (1966), and the flow within the narrow gap between rotating cylinders (Chandrasekhar 1961*a*, p. 298). Debler noted the correspondence between the two problems, and derived solutions for the thermal problem from Chandrasekhar's computations. Similarly, our own computations for marginal stability of the Poiseuille flow are directly comparable with those of Chandrasekhar. Certain asymptotic results and the principle of exchange of stabilities for the rotating cylinder case also apply directly to the problem under consideration.

The basic undisturbed velocity profile of plane Poiseuille flow is

$$U(y) = 6(y-y^2) \tag{22}$$

with velocity gradient

$$U'(y) = 6(1-2y). \tag{23}$$

Substituting (23) into (14) and combining with (15) results in the sixth-order disturbance equation

$$(D^2-\alpha^2-\sigma Re)^2(D^2-\alpha^2)\hat{v}+\alpha^2 4Re^2 Ro(3-Ro)\left(1-\frac{6}{3-Ro}y\right)\hat{v}=0, \tag{24}$$

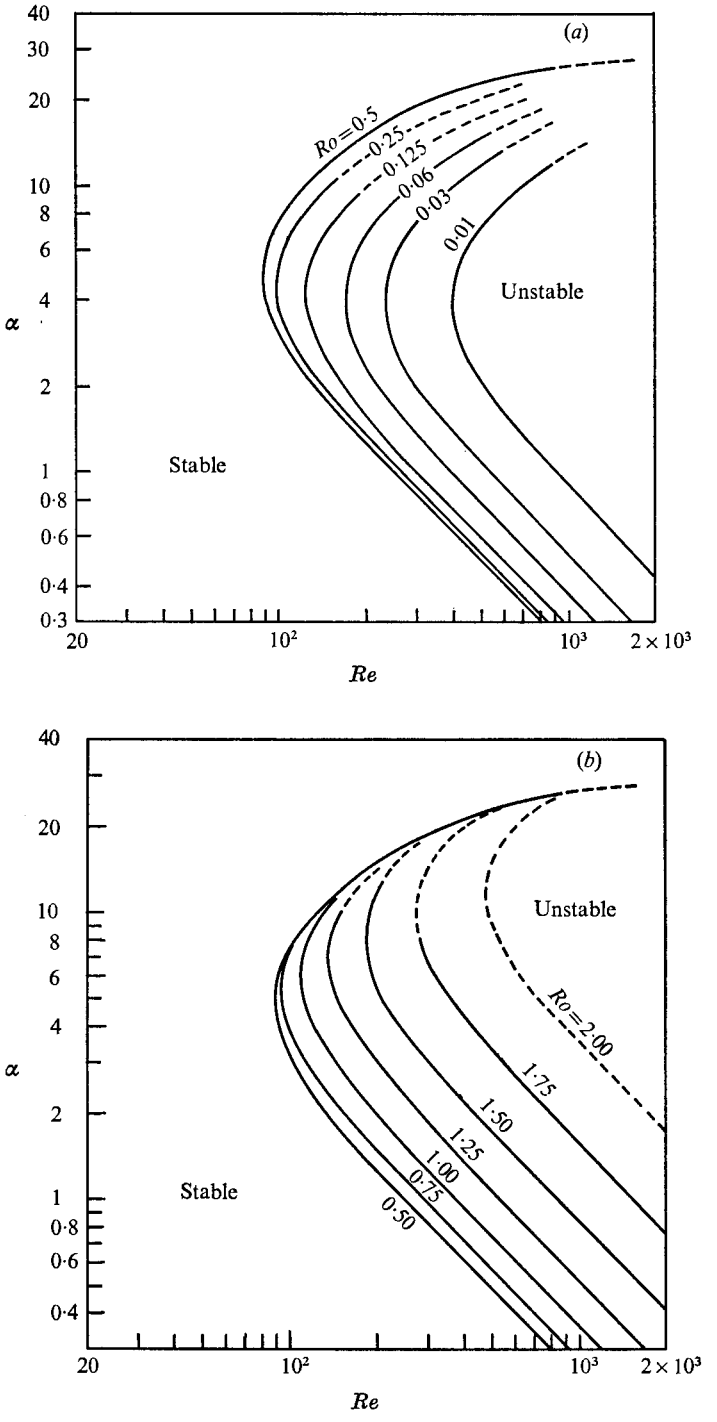

FIGURE 2. Neutral stability curves for laminar plane Poiseuille flow with rotation for (*a*) $Ro \leqslant 0{\cdot}5$, and (*b*) $Ro \geqslant 0{\cdot}5$.

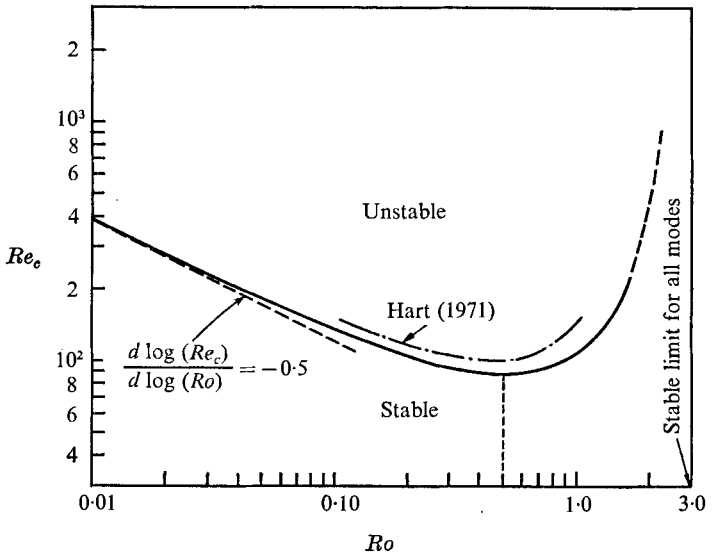

FIGURE 3. Critical Reynolds numbers for neutral stability in laminar plane Poiseuille flow.

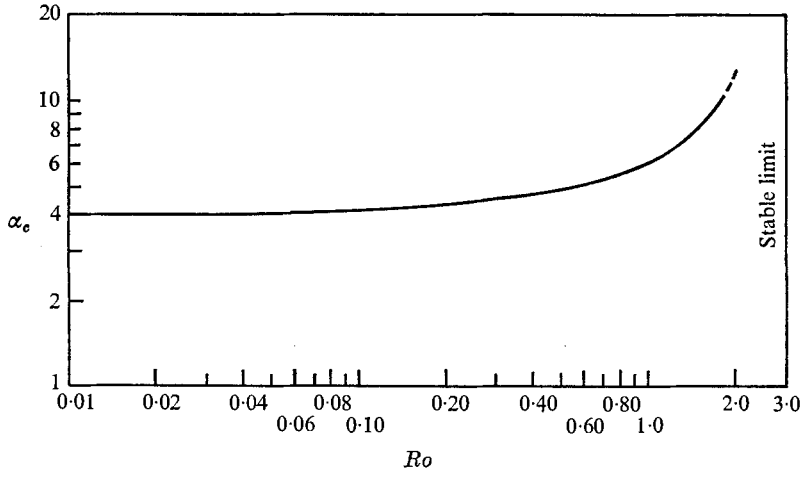

FIGURE 4. Critical cell frequency α_c for neutral stability in laminar plane Poiseuille flow.

which is arranged to emphasize the similarities with the disturbance equations of the analogous problems. The boundary conditions (18) remain unchanged. The equivalent differential equation for the rotating cylinder problem is obtained by combining the disturbance equations for the radial and tangential velocities given by Chandrasekhar (1961*a*, p. 299) into one differential equation for the eigenfunctions of the tangential velocity $\hat{v}(\zeta)$ with corresponding boundary conditions

$$(D^2-\alpha^2-\sigma)^2(D^2-\alpha^2)\tilde{v}+\alpha^2 Ta[1-(1-\mu)\zeta\}]\tilde{v}=0, \tag{25a}$$

$$\tilde{v}=D^2\tilde{v}=(D^2-\alpha^2-\sigma)D\tilde{v}=0, \quad \zeta=0,1. \tag{25b}$$

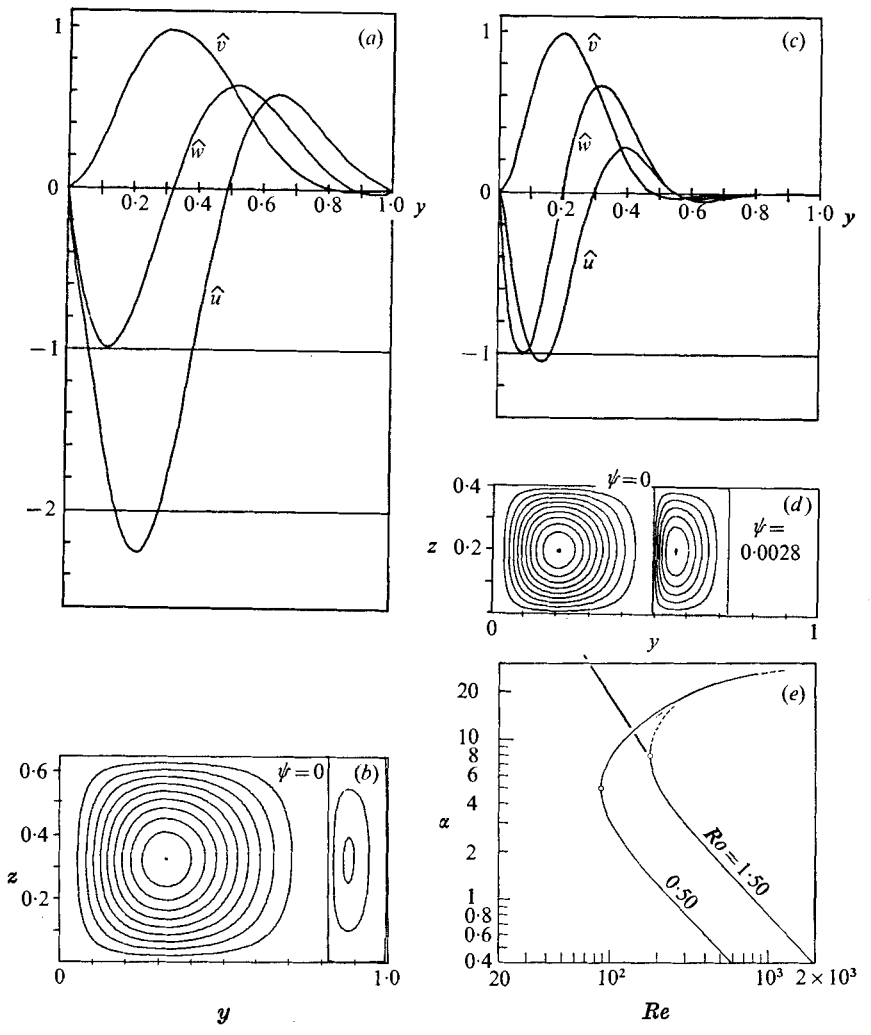

FIGURE 5. Stability in laminar plane Poiseuille flow. (*a*) Critical eigensolution, $Ro = 0{\cdot}5$, $Re_c = 88{\cdot}5$; (*b*) critical stream function, $\alpha = 4{\cdot}9$. In the left panel of (*b*), contours represent $\psi = 0{\cdot}1\ (0{\cdot}1)\ 1{\cdot}0$; in the right, $\psi = -0{\cdot}005, -0{\cdot}01$. (*c*) Critical eigensolution, $Ro = 1{\cdot}5$, $Re_c = 179{\cdot}2$; (*d*) critical stream function, $\alpha = 7{\cdot}8$. In the left panel of (*d*), contours represent $\psi = 0{\cdot}1\ (0{\cdot}1)\ 1{\cdot}0$; in the centre, $\psi = -0{\cdot}01\ (0{\cdot}005)\ -0{\cdot}03$. In (*e*), O indicates the two points associated with (*a*), (*b*) and (*c*), (*d*).

Ta is the Taylor number, μ the ratio of the angular velocities of the two cylinders, and ζ is the normalized radial co-ordinate measured from the inner cylinder toward the outer one.

The similarity of (24) to (25*a*) for the marginal case ($\sigma = 0$) is immediately apparent, although the boundary conditions do not appear to bear this same characteristic. In spite of this, the analogy remains intact. Following a straightforward analysis of adjoint differential systems by Chandrasekhar (1961*b*), one can show that the two problems are adjoint (i.e. the characteristic equations

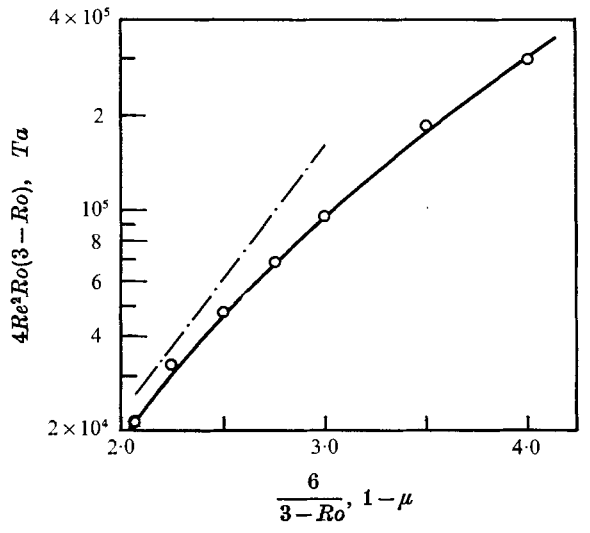

FIGURE 6. Solutions for neutrally stable roll-cell disturbances between rotating cylinders and in rotating plane Poiseuille flow; ○, laminar Poiseuille flow, present calculations; —·—, Hart (1971); ——, Taylor problem, Chandrasekhar (1961*b*).

for Ta and $4Re^2Ro(3-Ro)$ are transposes of each other), thus having the same eigenvalues. In terms of the analogy, then, the two problems yield the same values for the critical cell frequencies α_c, when, simultaneously,

$$4Re^2Ro(3-Ro) = Ta \quad \text{and} \quad 6/(3-Ro) = 1-\mu. \qquad (26), (27)$$

Before discussing neutrally stable solutions, we shall briefly consider the validity of the principle of exchange of stabilities for this case. Because of the variable coefficient in (24), the disturbance equations are not self-adjoint, and the usual proof that the eigensolutions admit only real values of σ cannot be carried through. Chandrasekhar concluded, however, that, since the characteristic values for the rotating cylinder problem are nearly independent of $1-\mu$, exchange of stabilities is satisfied in the narrow-gap approximation of the rotating cylinder case. Thus, the mathematical correspondence between the disturbance equations (24) and (25) leads to the same conclusion with respect to the neutral state of rotating Poiseuille flow.

Neutrally stable solutions of (24), (18) within the admissible range of Ro have been computed numerically for various values of the cell number α. (For details of the numerical procedure, see Lezius 1975.) As illustrated in figure 2, a large range of marginally stable cell modes results for given Re or Ro. In an experiment, however, only the critical, or most unstable, modes are usually observed. These occur at the lowest Reynolds number, along the stability boundary, for each selected value of Ro. The critical states are summarized in one curve in figure 3. It is noted that the lowest critical Reynolds number ($Re_c = 88{\cdot}53$) occurs at $Ro = 0{\cdot}5$. In the limit $Ro \to 0$, $Re_c \sim Ro^{-\frac{1}{2}}$. This result obtains directly by analogy, from the critical Taylor number for $\mu = -1$, $Ta_c = 1{\cdot}868 \times 10^4$, and from the fact that in the regime of small rotations α_c is independent of Ro. (See figure 4.)

Limiting values for Re_c and α_c as $Ro \to 3$ are also derived by analogy from Chandrasekhar's asymptotic solutions for $(1-\mu) \to \infty$:

$$Ta_c \sim (1-\mu)^4 \quad \text{and} \quad \alpha_c \sim (1-\mu).$$

Substitution from (26) and (27) yields

$$Re_c \sim (3-Ro)^{-\frac{1}{2}} \quad \text{and} \quad \alpha_c \sim (3-Ro)^{-1}.$$

As $Ro \to 3$, the layer of negative vorticity vanishes at the $y = 0$ boundary, leaving the entire fluid in a stabilized state. Marginal stability in this limit requires infinite Coriolis forces, as indicated in figure 3 by the asymptotic trend of Re_c.

Critical eigenfunctions and stream functions of the induced cellular flow are shown in figure 5 for $Ro = 0{\cdot}5$ and $1{\cdot}5$, respectively. The most critical disturbance mode $\alpha_c = 4{\cdot}9$ has a spanwise cell thickness (half-period) of approximately $0{\cdot}64$ times the channel width.

Direct comparison of our finite-difference solutions with Chandrasekhar's series approximations is made in figure 6. Also shown are the solutions by Hart (1971),† which were obtained by the Galerkin method. The differences in the numerical results are believed to arise from the singular nature of the disturbance equations. Chandrasekhar noted that, for $\mu < -3$, solutions of acceptable accuracy would require an increasing number of approximations. In our own computations, numerical difficulties developed when $\alpha > 8$ and $Ro > 1{\cdot}5$. In the range of small Ro, numerical instabilities occurred when $\alpha > 15$.

4. Two-layer model of turbulent flow

Certain assumptions and simplifications need to be made before the neutral stability of turbulent flow can be examined. For one, the existence of a neutral state in the conventional sense is rather questionable. Experimentally, it is quite difficult to detect the exact point of onset of instabilities in a flow with turbulent fluctuations much larger in magnitude than the initial disturbance amplitude. On the other hand, our observations of stable and unstable states, reported in Johnston *et al.* (1972), imply at least the existence of a transition regime which can be assumed equivalent to the neutral state. In carrying out an analysis such as was done for the laminar flow, a realistic description of the turbulent mean flow properties must include the effects of rotation not present in the laminar case. These are the asymmetry of the mean velocity profile, and the contribution of an apparent eddy viscosity ν_t to turbulent stresses that are expected to inhibit formation of the instability. As indicated by the general disturbance equations (14) and (15), these features of mean flow enter into the analysis through the mean velocity gradient of the turbulent flow U_t', and through the Reynolds number.

† Hart's solutions were originally presented in terms of the Rossby number ($0{\cdot}75\ Ro^{-1}$) and the Ekman number ($0{\cdot}5\ Re^{-1}Ro^{-1}$). They have been transformed to conform to the non-dimensional parameters chosen here.

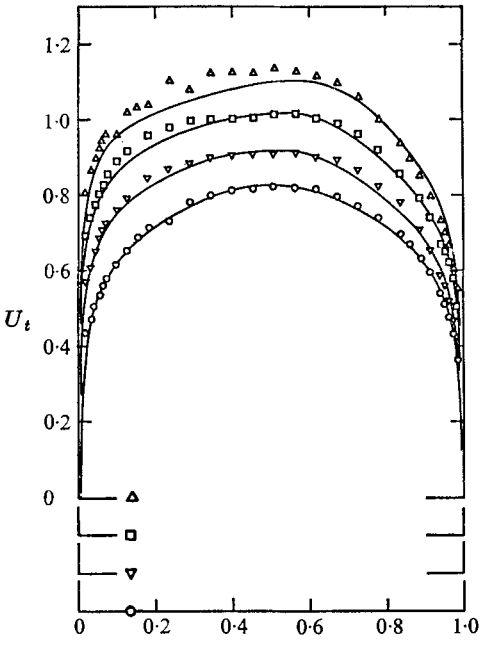

FIGURE 7

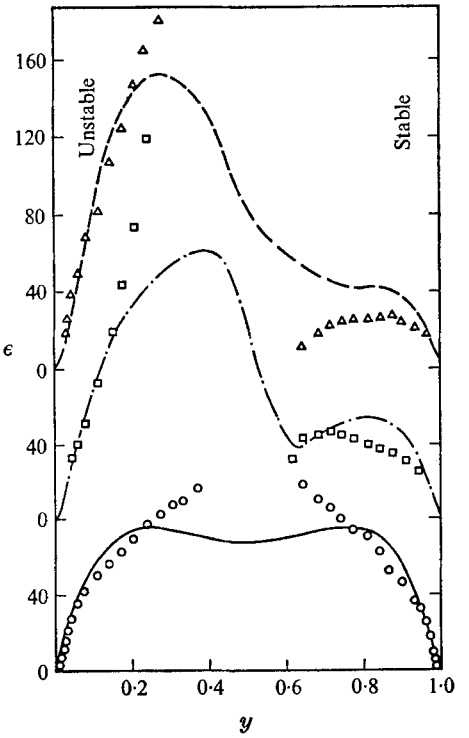

FIGURE 8

FIGURE 7. Comparison of predicted turbulent mean velocity profiles (——) with measurements (symbols) by Halleen & Johnston (1967), for rotating channel flow. $U_t = \bar{U}_t/U_m$, $A^+ = 29$, $\kappa = 0{\cdot}45$, $\beta = 4$.

Re	35200	35400	35300	35800
Ro	0	0·027	0·042	0·082
	—○—	—▽—	—□—	—△—

FIGURE 8. Comparison of experimentally deduced (symbols) with predicted (A7) eddy viscosity profiles. $\epsilon = 1 + \nu_t(y)/\nu$, $At = 29$, $\kappa = 0{\cdot}45$, $\beta = 4$

Re	35300	35300	35800
Ro	0·042	0·042	0·082
	—○—	—·—□—·—	——△——

A semi-empirical prediction scheme for the asymmetrical turbulent mean flow with rotation was reported in Lezius & Johnston (1971), where velocity profiles were computed for the Reynolds numbers and levels of rotation *Ro* investigated experimentally by Halleen & Johnston (1967). The agreement of the velocity measurements (reported in Johnston *et al.* 1972) with the predicted profiles is shown in figure 7 for the case $Re \approx 35000$. Similar agreement was obtained with velocity profiles measured at $Re \approx 11400$ and $0 \leqslant Ro \leqslant 0{\cdot}117$. The equations of turbulent mean motion were closed with a modified version of the Cess (1958) eddy viscosity model for channel flow, to account for the asymmetrical effects of Coriolis forces upon the production of turbulent stresses in the stabilized and destabilized flow regions. (See appendix.) In figure 8, we compare eddy viscosity

profiles deduced from experimental data with those computed (A 7) for the velocity profiles shown in figure 7. It is noted that the general rise of eddy viscosity with Reynolds number is accompanied by large stabilizing and destabilizing effects of rotation, which locally reduce or increase ϵ correspondingly, via the direct effect of mean rotation upon local rate of turbulence production. For detailed discussion of these effects, the reader is referenced to Lezius & Johnston (1971) and Johnston *et al.* (1972).

Although $U_t'(y)$ and $\nu_t(y)/\nu$ are known numerically, we cannot immediately proceed with the stability analysis, since (17) and (18) were derived for a constant viscosity coefficient. Retaining variable eddy viscosity, on the other hand, would not only increase the complexity of the disturbance equations considerably, but also introduce new uncertainties by requiring higher-order derivatives of $\nu_t(y)/\nu$. Considerable simplification of the stability problem is thus achieved by assuming that the fluid is composed of two layers, whereby in each layer, the effects of eddy viscosity are represented by the integrated average of $\nu_t(y)/\nu$ over the layer thickness. The model therefore implies physically that at onset of instabilities, the destabilizing inertial stresses due to Coriolis forces are balanced by a corresponding average of the turbulent stresses in the layer. This assumption appears reasonable since the disturbance spans essentially the entire layer thickness. Hence, we define the total viscosity ratios

$$\left.\begin{aligned} \epsilon_1 &\equiv 1+\frac{\bar{\nu}_{t1}}{\nu} = 1+\frac{1}{\nu y_1}\int_0^{y_1}\nu_t(y)\,dy, \\ \epsilon_2 &\equiv 1+\frac{\bar{\nu}_{t2}}{\nu} = 1+\frac{1}{\nu(1-y_1)}\int_{y_1}^{1}\nu_t(y)\,dy. \end{aligned}\right\} \tag{28}$$

In figure 9, the corresponding average values ϵ_1 and ϵ_2 of the two-layer model are indicated with respect to the computed distribution of $\epsilon(y)$ for the case of $Re = 35200$, $Ro = 0{\cdot}042$. The plane y_1 that divides the two layers is located where the slope of the predicted mean velocity profile is zero. Although $\epsilon_{1,2}$ is discontinuous at y_1, the turbulent mean shear stress remains continuous, because at this point $U_t' = 0$.

The effects of turbulent friction enter into the analysis through the Reynolds number; and, having absorbed these effects in $\epsilon_{1,2}$, we can now define equivalent turbulent Reynolds numbers for the unstable and stable regions, respectively:

$$Re_{t1,2} = U_m 2D/(\nu+\bar{\nu}_{t1,2}) = Re/\epsilon_{1,2}.$$

The disturbance equations (14)–(16) are thus combined, to give

$$\left(D^2-\alpha^2-\sigma\frac{Re}{\epsilon_{1,2}}\right)^2(D^2-\alpha^2)\hat{v}(y)+\frac{\alpha^2 2Re^2Ro}{\epsilon_{1,2}^2}(U_t'-2Ro)\hat{v}(y) = 0, \tag{29}$$

$$\hat{v} = D\hat{v} = \left(D^2-2\alpha^2-\sigma\frac{Re}{\epsilon_{1,2}}\right)D^2\hat{v} = 0, \quad y = 0, \quad y = 1. \tag{30}$$

It is seen that, for this two-layer model with piecewise constant ϵ, the disturbance equations are essentially identical to those for laminar flow, although they retain the salient features of the turbulent mean velocity profile and the difference

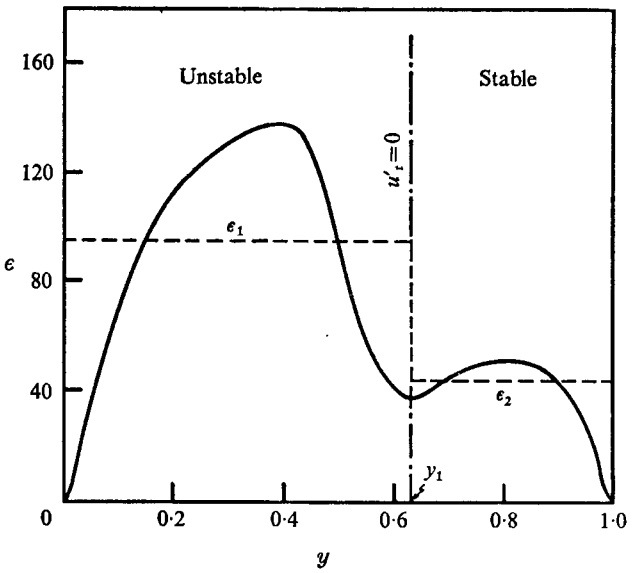

FIGURE 9. Definition of average total viscosity for two layer model of rotating, turbulent channel flow. $\epsilon(y) = 1 + \nu_t(y)/\nu$ calculated for $Re = 35300$ and $Ro = 0{\cdot}042$.

in total viscosity in the stable and unstable regions. Equation (29) clearly indicates the strong damping character that is contributed by the turbulent viscosity. The effect of increasing ϵ, as the flow is rendered more turbulent at larger Reynolds numbers, will be to delay the onset of instabilities to considerably higher values of critical Ro than would be predicted by using the laminar viscosity alone. This point will be discussed further when we consider the physical importance of the turbulent Reynolds number in connexion with the numerical results. It should also be pointed out that the stability of the flow will be influenced by the fact that the mean vorticity $-(U' - 2Ro)$ is no longer a linear relationship in y, as was the case for laminar flow, but depends in a complicated manner upon Re and Ro.

Numerical solutions for the onset of instabilities ($\sigma = 0$) were initiated by first computing profiles of $U'_t(y)$ and of the average total viscosities ϵ_1 and ϵ_2. (See appendix, (A 1).) Subsequently, solution of the disturbance equations followed along the same lines as for the laminar case. The results of these computations for Reynolds numbers ranging from 2000 to 35000 are shown in figure 10; the corresponding critical rotation numbers Ro_c and spanwise cell numbers α_c are listed in table 1. It is interesting to note that the predicted onset of instabilities in fully-turbulent flow ($Re > 6000$) is restricted to a narrow range of critical rotation numbers near $Ro_c \leqslant 0{\cdot}022$, which is in good agreement with experimental observations reported in detail in Johnston *et al.* (1972). These studies indicated that the appearance of the roll-cell structure as an instability of the rotating flow was essentially independent of the Reynolds number. Below $Ro \approx 0{\cdot}02$, roll cells could not be detected by means of flow visualization, but they were regularly observed at $Ro > 0{\cdot}04$. This result is readily explained by remembering that the

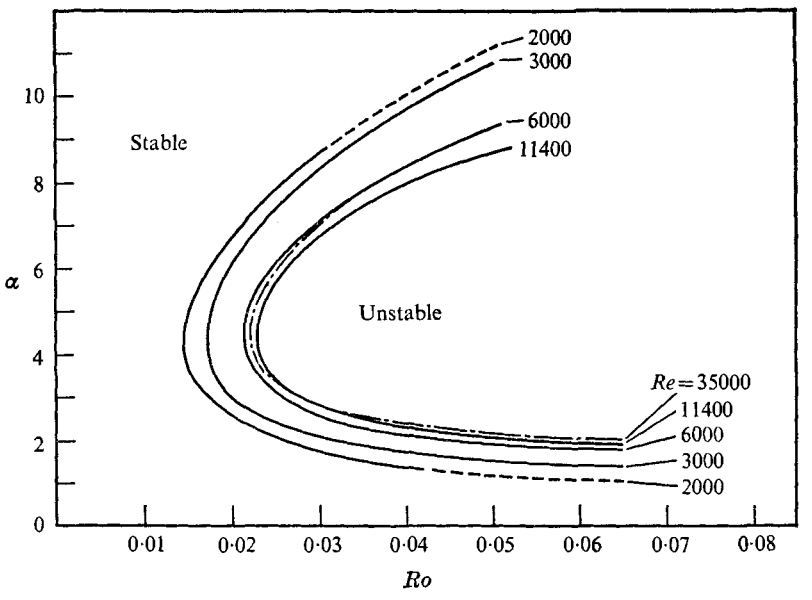

FIGURE 10. Neutral stability curves for roll-cell instabilities in rotating turbulent channel flow.

Re	Ro_c	α_c	ϵ_1	ϵ_2	Re_{t1}	Re_{t2}	$\frac{2Re^2Ro}{\epsilon_1^2}$
2000	0·0152	4·25	5·68	3·74	352·1	534·8	3769
3000	0·0174	4·30	8·69	5·35	345·2	560·8	4147
6000	0·0216	4·40	17·65	9·98	339·9	601·2	4991
11400	0·0230	4·35	32·51	17·65	350·7	645·9	5658
35000	0·0223	4·50	90·01	48·04	388·8	728·6	6742

TABLE 1. Critical parameters for onset of roll instabilities in rotating turbulent channel flow

effect of fluid friction upon the analogous thermal convection instabilities is one of pure damping. In a similar manner, turbulent friction intensifies the resistance of the rotating flow to roll-cell instabilities. For instance, inspection of table 1 shows that, over the range of $6000 < Re < 35000$, ϵ_1 increases proportionally with Re, thus causing only a small variation in the physically meaningful Reynolds number of the turbulent flow Re_{t1}. In fact, within the range of the fully-turbulent regime, we find that

$$345 < Re_{t1} = Re/\epsilon_1 < 390.$$

Considering the close agreement with the visual studies, it is reasonable to conclude that, in the experiments, the increased Coriolis forces at higher Re were offset by correspondingly larger friction forces, attributable to turbulence intensity. Since the stabilized opposite fluid layer makes only a negligible contribution in counteracting instabilities, the magnitude of ϵ_2 is of little consequence.

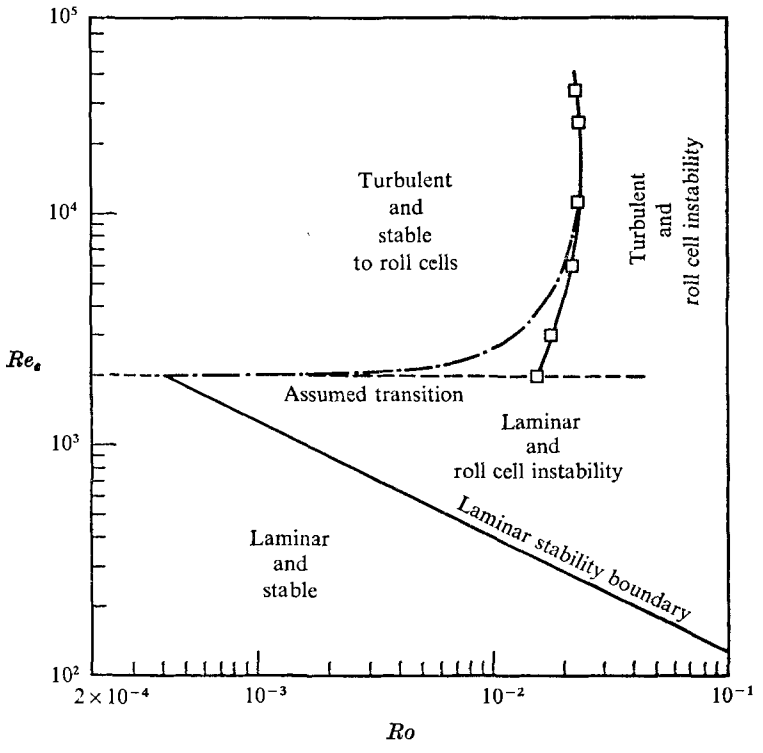

FIGURE 11. Neutral stability boundary for laminar Poiseuille and turbulent channel flow (two-layer model). □, calculated neutral states; —·—·—, estimated neutral states.

Although in the transition from laminar to turbulent flow $Re \to 2000$ the results should approach those obtained for Poiseuille flow ($Re_c \approx 0{\cdot}0004$) with $Re_t \to Re$, the computations of $\epsilon_{1,2}$ showed that the Cess eddy viscosity (appendix, (A 3)) does not vanish properly in this limit. For example, at the transitional Reynolds number $Re = 2000$, we have from table 1 $\epsilon_1 \approx 5{\cdot}7$ and $Re_{t1} \approx 352$, indicating a turbulent flow. This shortcoming is reflected in the computed onset of instabilities at $Ro_c \approx 0{\cdot}015$.

The stability boundary separating the stable and unstable states in laminar and turbulent flow is shown in figure 11. Because of the uncertainty in determining the magnitude of ν_t in the transition regime, we can presently only guess the location of the neutral boundary in this region.

Computed eigenfunctions and stream functions for the case $Re = 35000$ are shown in figure 12. As a consequence of the constant eddy viscosity model, they bear close resemblance to the critical eigensolutions for the laminar case. A typical example of the actually observed cellular flow patterns at rotation numbers much larger than Ro_c is depicted in figure 13 (plate 1). In this end-view photograph (the mean flow is out of the picture plane), the disturbance flow is indicated by the deformation of an originally straight hydrogen bubble time line. Although periodic, the instability does not exhibit the linear characteristic (i.e. spanwise sinusoidal variation) originally assumed in the analysis. Examination

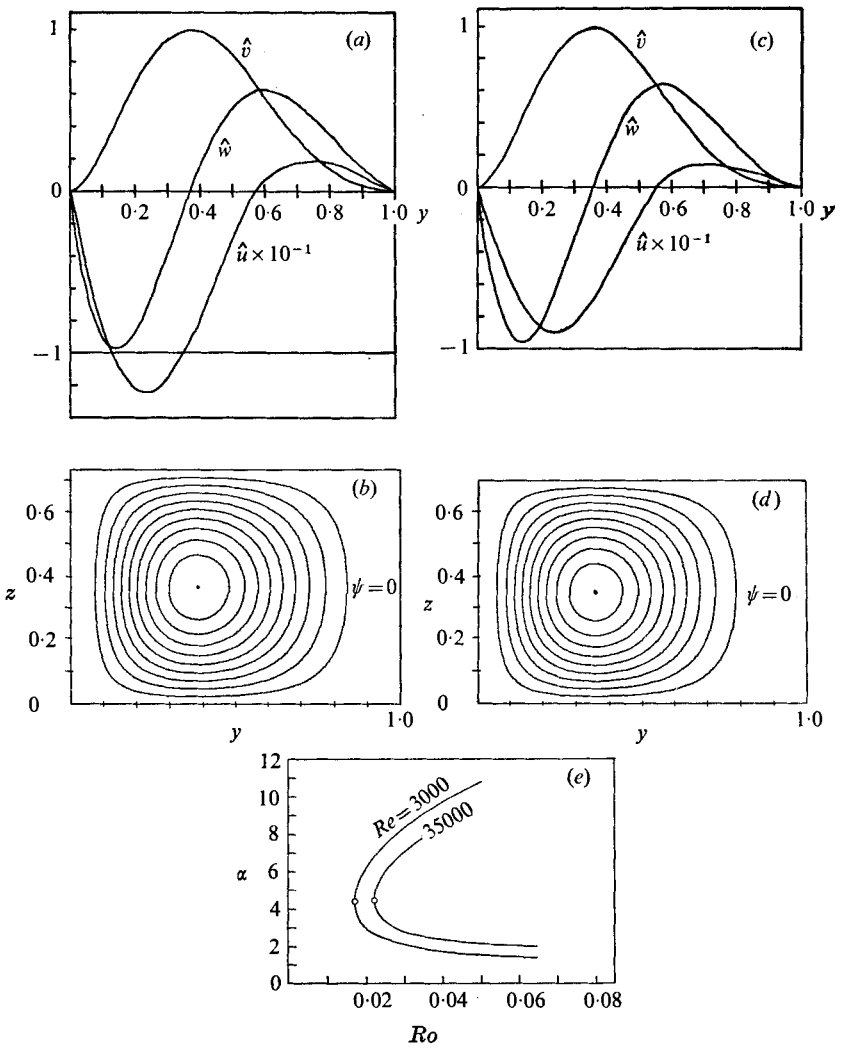

FIGURE 12. Roll-cell instabilities in turbulent channel flow (two layer model). (*a*) Critical eigensolution, $Ro_c = 0{\cdot}0174$, $Re = 3000$; (*b*) critical stream function, $\alpha = 4{\cdot}3$. Contours represent $\psi = 0{\cdot}1$ (0·1) 1·0. (*c*) Critical eigensolution, $Ro_c = 0{\cdot}0223$, $Re = 35000$; (*b*) critical stream function, $\alpha = 4{\cdot}5$. Contours represent $\psi = 0{\cdot}1$ (0·1) 1·0. In (*e*), ○ indicates the two points associated with (*a*), (*b*) and (*c*), (*d*).

of many such photographs revealed that, at high *Ro*, the cell centres tend to gravitate toward each other when the secondary flow between them is away from the wall. The motion picture films from which figure 13 was reproduced showed clearly that the wall fluid is essentially ejected through more or less regularly spaced narrows gaps in the overlying fluid layer that is forced toward the unstable wall by the mean Coriolis field. The resulting irregular spanwise variation of the induced flow is attributed to strong nonlinear interaction between the turbulent mean flow and the disturbance. At high *Ro*, these flow components are of comparable magnitude in the wall region. Although the supercritical dis-

turbance flow shown in figure 13 is clearly outside the validity of linear stability analysis, the average cell number $\alpha \approx 5$ of the two cells compares favourably with the predicted value of $\alpha \approx 4{\cdot}4$. Over the experimentally investigated range of Re and Ro, furthermore, the observed spanwise cell separations vary between $\alpha \approx 4{\cdot}5$ and $\alpha \approx 6$, whereby the higher values apparently result at rotation rates considerably larger than Ro_c. The general agreement, then, between predicted and observed conditions for instabilities indicates that, despite the difficulty in detecting and observing the critical state experimentally in a turbulent flow, the sinusoidal spanwise cell variation may be considered a valid assumption for describing the instability at the point of onset.

5. Conclusions

We have considered the effects of Coriolis forces in rotating laminar and turbulent channel flow with respect to longitudinal roll-cell disturbances of the Taylor type. Analogies to the disturbance equations for buoyancy-driven convection and classical Taylor instabilities provide immediate solutions for the marginal stability of two types of laminar plane flow considered. Couette flow with rotation in a direction opposite to the absolute vorticity of the fluid is dynamically analogous to Bénard convection and to the differentially heated Couette flow. As in the analogous cases, marginal stability is found when the parameter

$$4Re^2Ro(1-Ro)$$

assumes the value of the critical Rayleigh number $Ra_c = 1708$; hence, the range of instability lies in $0 < Ro < 1$.

For the disturbance equations of laminar plane Poiseuille flow in rotation, we find analogous counterparts in the equations describing hydrodynamic instability of the internally heated fluid layer, and of the flow within a narrow gap between rotating cylinders. Marginally stable solutions for roll-cell disturbances can be derived from Chandrasekhar's solutions for the rotating cylinder problem by setting the stability parameter for Poiseuille flow equal to the Taylor number: $4Re^2Ro(3-Ro) = Ta$. The requirement $Ta > 0$ then limits instabilities to the range $0 < Ro < 3$, independent of the sign of the rotation. Below the calculated critical Reynolds numbers, however, the flow is stable with respect to all disturbance modes.

The complexities of turbulent flow require several assumptions, in order to keep the disturbance equations in a tractable form. To this end, a two-layer model, with a constant eddy viscosity in each layer, appears to afford a sufficient degree of simplification. The resulting quasi-linear description of the turbulent mean flow, nevertheless, incorporates a physically accurate velocity profile and average eddy viscosity levels that are apparently representative of the effects of turbulent friction in the stable and unstable fluid layers. The numerical solutions predict onset of instabilities above $Ro \approx 0{\cdot}02$ for channel Reynolds numbers between 6000 and 35000. These values agree quite closely with the experimental observations.

We gratefully acknowledge the support of our work by the Mechanics Section of the Engineering Division of the National Science Foundation. This paper was prepared under NSF grant GK-16450. In addition, we thank Professor Acrivos and Professor Reynolds for their many helpful comments and criticisms.

Appendix

Turbulent mean velocity profiles are computed by integrating an expression for the mean profile gradient

$$U_t'(y) = \tfrac{1}{2} Re B_0 \frac{(1 + m Ro - 2y)}{[1 + \nu_{t_0}(y)/\nu] f(\beta, Ri)}, \tag{A 1a}$$

subject to the continuity condition

$$\int_0^1 U_t(y)\, dy = 1. \tag{A 1b}$$

Equation (A 1) is derived from the assumption that, in fully-developed turbulent channel flow, the turbulent mean shear stress τ varies linearly between walls. Hence,

$$\frac{d\tau}{dy} = \frac{d}{dy}\left[\left(1 + \frac{\nu_{t_0}(y)}{\nu}\right)\frac{dU_t}{dy}\right] = -Re B_0. \tag{A 2}$$

B_0 is the non-dimensional shear stress gradient without rotation. Rotational effects upon wall shear stresses are accounted for by the factor $m Ro$.

The Cess (1958) eddy viscosity without rotation is given by

$$\frac{\nu_{t_0}(y)}{\nu} = \tfrac{1}{2}\left[1 + \frac{\kappa^2 Re^2 B_0^2}{72} F^2(y)\left\{1 - \exp\left(-\frac{Re(\frac{1}{2}B_0)^{\frac{1}{2}}}{A^+} y\right)\right\}^2\right]^{\frac{1}{2}} - \tfrac{1}{2}. \tag{A 3}$$

For two-dimensional channel geometry,

$$F(y) = 4(y - y^2)(3 - 8y - 8y^2). \tag{A 4}$$

$\kappa = 0{\cdot}45$ and $A^+ = 29$ are the applicable von Kármán constant and sublayer thickness parameter, respectively.

Local effects of rotation upon total viscosity are a function of the local Richardson number Ri, as expressed by the Monin–Oboukhov formula

$$f(\beta, Ri) = (1 + \beta Ri)^{-1}. \tag{A 5}$$

(See Bradshaw 1969.) $\beta = 4$ is an empirical parameter that influences the profile shape of $U_t(y)$. As in buoyancy-driven flows, the Richardson number provides a measure of local fluid stability. In rotating channel flow, therefore,

$$Ri \equiv -2Ro(U_t' - 2Ro)/(U_t')^2. \tag{A 6}$$

In order to avoid numerical difficulties when (A 1) is integrated iteratively, it is necessary to redefine Ri in the central flow region so that

$$Ri = 0 \quad \text{when} \quad U_t' = 0.$$

Predicted mean velocity profiles are compared with experimental measurements in Lezius & Johnston (1971).

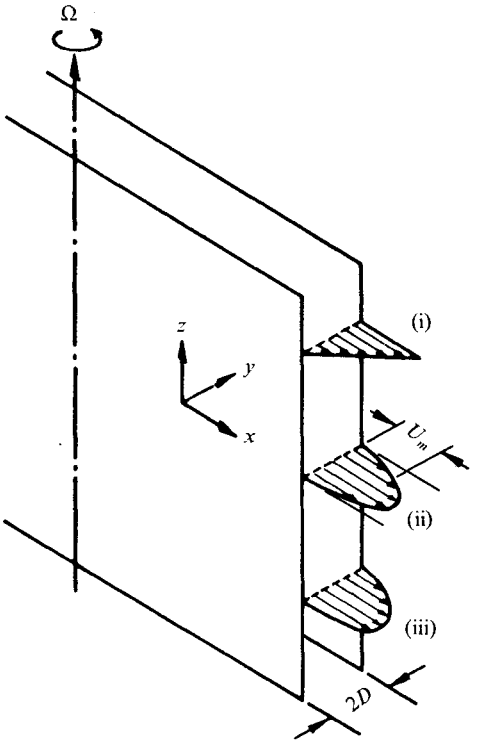

FIGURE 14. Co-ordinates and velocity profiles in plane, rotating channel flow: (i) plane Couette flow; (ii) plane Poiseuille flow; (iii) turbulent channel flow.

In the stability analysis we let, for convenience,

$$1+\nu_t(y)/\nu = (1+\nu_{t_0}(y)/\nu)f(\beta, Ri). \tag{A 7}$$

(See equation (28).) For, except in the extremely thin laminar sublayer

$$(\delta_{\text{lam}}/2D \approx 5\times 10^{-4}), \quad \nu_t(y)/\nu \gg 1.$$

REFERENCES

BRADSHAW, P. 1969 The analogy between streamline curvature and buoyancy in turbulent shear flow. *J. Fluid Mech.* **36**, 177.

CESS, R. D. 1958 A survey of the literature on heat transfer in turbulent tube flow. Thesis, University of Pittsburgh, Pennsylvania.

CHANDRASEKHAR, S. 1961*a* *Hydrodynamic and Hydromagnetic Stability*. Oxford University Press.

CHANDRASEKHAR, S. 1961*b* Adioint differential systems in the theory of hydrodynamic stability. *J. Math. Mech.* **10**, 683.

DEBLER, W. R. 1966 On the analogy between thermal and rotational hydrodynamic stability. *J. Fluid Mech.* **24**, 165.

HALLEEN, R. M. & JOHNSTON, J. P. 1967 The influence of rotation on flow in a long rectangular channel: an experimental study. *Department of Mechanical Engineering, Stanford University, Rep. MD-18.*

HART, J. E. 1971 Instability and secondary motion in a rotating channel flow. *J. Fluid Mech.* **45**, 341.

HUNG, W. L., JOSEPH, D. D. & MUNSON, B. R. 1972 Global stability of spiral flow. Part 2. *J. Fluid Mech.* **51**, 593.

JOHNSTON, J. P., HALLEEN, R. M. & LEZIUS, D. K. 1972 Effects of spanwise rotation on the structure of two-dimensional fully developed turbulent channel flow. *J. Fluid Mech.* **56**, 533.

JOSEPH, D. D. 1966 Nonlinear stability of the Boussinesq equations by the method of energy. *Arch. Rat. Mech. Anal.* **22**, 163.

LEZIUS, D. K. 1975 Finite difference solutions of Taylor instabilities in viscous plane flow. *Computers & Fluids*, **3**, 103.

LEZIUS, D. K. & JOHNSTON, J. P. 1971 The structure and stability of turbulent wall layers in rotating channel flow. *Department of Mechanical Engineering, Stanford University, Rep. MD*-29.

PEDLEY, T. J. 1969 On the instability of viscous flow in a rapidly rotating pipe. *J. Fluid Mech.* **35**, 97.

PELLEW, A. & SOUTHWELL, R. V. 1940 On maintaining a convective motion in a fluid heated from below. *Proc. Roy. Soc.* A**176**, 312.

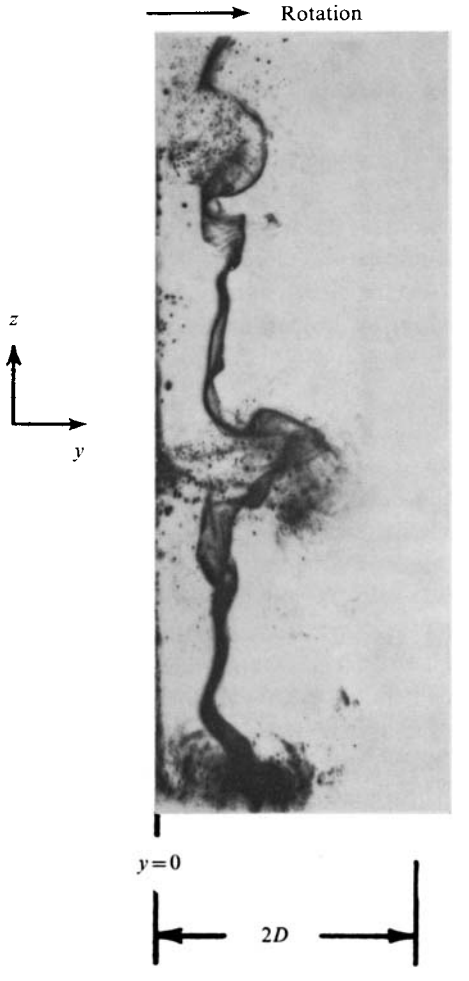

FIGURE 13. End-view photograph of roll-cell instabilities in rotating turbulent channel flow, $Re = 5900$, $Ro = 0{\cdot}32$.